Journal of Magnetics 10(3), 103-107 (2005)

# Room-temperature Magnetotransport in Degenerately Doped GaAs:(Mn,Be) by Virtue of the Embedded Ferromagnetic Clusters

**Fu Cheng Yu, Dojin Kim*, Hyojin Kim, and Young Eon Ihm**

*Department of Materials Science and Engineering, Chungnam National University, Daejeon 305-764, Korea*

(Received 10 August 2005)

**Magnetotransport is a prerequisite to realization of electronic operation of spintronic devices and it would be more useful if realized at room temperature. The effects of Be codoping on GaMnAs on magnetotransport were investigated. Mn flux was varied for growth of precipitated GaMnAs layers under a Be flux for degenerate doping via low-temperature molecular beam epitaxy. Magnetotransport as well as ferromagnetism at room temperature were realized in the precipitated GaAs:(Mn,Be) layers. Codoping of Be was shown to promote formation of MnGa clusters, and annealing process further stabilized the cluster phases. The room-temperature magnetic properties of the layers originate from the ferromagnetic clusters of MnGa and MnAs embedded in GaAs. The degenerately doped metallic GaAs matrix allowed the visualization of the magnetotransport through anomalous Hall effect.**

**Key words :** GaMnAs, Be codoping, Cluster

## 1. Introduction

III-V ferromagnetic semiconductor has attracted great attention due to potential application to spintronics since a successful demonstration of spin injection from ferromagnetic GaMnAs into semiconductor [1]. GaMnAs is the most intensively explored III-V ferromagnetic semiconductor by Ohno group [2-5] and others [6-8]. According to the theory by Dietl *et al.* [9], the Curie temperature (Tc) of magnetic semiconductors can be enhanced with higher incorporation of magnetic element and accompanying high carrier concentration. Low-temperature molecular beam epitaxy (MBE) technique has been successful for GaMnAs growth, but the maximum Tc was limited to ~110 K at ~5% Mn. Higher Mn incorporations produced MnAs precipitates, and which has lowered the Curie temperature. Recently, it was shown that Be codoping on GaMnAs affects Tc [10, 11]. In those studies, while the Be-codoping effect on Tc enhancement was controversial, the discussion was on the solid solution type GaMnAs structures.

In the meantime, the authors have shown that another III-V system of GaMnN reveals room temperature ferromagnetism in the structures grown by MBE using a single GaN precursor. A metallic GaMnN layer revealed a room-temperature magnetotransport, and which was realized through the segregation of highly conductive paramagnetic $Mn_3GaN$ phase [12]. In the subsequent attempt to co-dope Mg into the matrix of GaMnN solid solution [13, 14], a dramatic enhancement in the saturation magnetization was realized, but magnetotransport phenomena could not be observed probably because of the far high resistance of the matrix with respect to the magnetoresistance effect. Both results suggest the importance of degenerate doping for observation of magnetotransport because the relatively small magnetotransport component may be easily buried under the high resistivity of the matrix. Detection of spin transport is crucial and prerequisite for electronically operating spin injection devices, particularly at room temperature from the economical point of view. In this study, we report an investigation of degenerately Be-codoped metallic GaMnAs layers pursuing room temperature magnetotransport. Ferromagnetic clusters embedded in highly conductive layer were shown to reveal magnetotransport.

## 2. Experiment

GaAs:Mn and GaAs:(Mn,Be) films were grown on

*Corresponding author: Tel: +82-42-821-6639,
Fax: +82-42-823-4224, e-mail: dojin@cnu.ac.kr

semi-insulating GaAs (100) substrates via solid-source MBE. The background pressure with flowing liquid nitrogen was at low $10^{-10}$ torr ranges. The substrates were firstly deoxidized at ~610 °C, and then ~300 nm thick GaAs buffer layer was grown at 580 °C at a growth rate of 0.5 $\mu$m/hr. The substrate temperature was then lowered to ~300 °C under arsenic flux for low-temperature growths of GaAs:Be, GaAs:Mn, and GaAs:(Mn,Be). The growth rate was also reduced down to 0.25 mm/hr. The employed $As_4$ pressure was ~$1.4 \times 10^{-6}$ torr. The detail of the MBE growth is described in Ref. 15. The Be flux was fixed at $T_{Be}$ = 1250 °C for metallic resistivity of the layers. The Mn cell temperature was varied for the growths of GaAs:Mn and GaAs:(Mn,Be) layers in the range of 850~910 °C, which covers the flux transition from homogeneous to precipitated GaMnAs layers. The GaAs:Mn and GaAs:(Mn,Be) layers will be called M- and BM-series, respectively, and each sample in each series is distinguished by the Mn cell temperatures.

The atomic concentration of Mn was measured by electron probe x-ray microanalysis (EPMA). The electrical and magnetic properties were investigated by temperature dependent resistivity measurement on van der Pauw geometry and superconducting quantum interference device (SQUID). The heat treatments of the structures at 900 °C for 30 sec using rapid thermal annealing in Ar ambient were also carried out, and their effects on the properties were examined.

## 3. Results and Discussion

DCXRD analysis shows the shoulder peak corresponding to the solid solution GaMnAs disappears as the second phases such as MnAs begins to form at high Mn incorporation [15, 16]. In the M-series, GaMnAs solid solution could form till the Mn flux for $T_{Mn}$=890 °C as revealed by the shoulder peak at GaAs (004), but the Mn-related precipitates as well has begun to form at this Mn flux. Therefore, the $T_{Mn}$=890 °C is the critical Mn cell temperature for precipitation in the M-series. On the other hand, when the Mn flux was varied under the given flux of Be ($T_{Be}$=1250 °C), the shoulder peaks are not seen at all the Mn flux ($T_{Mn}$=850~910 °C). This suggests that Be flux accelerates segregation of the precipitates, particularly $Mn_xGa$, as will be seen. Some Mn-related peaks also appeared over $T_{Mn}$=890 °C, as also occurred in the M-series, but it was difficult to index each XRD peak uniquely to a precipitate. Nevertheless, they can be assigned to Mn, $Mn_xGa$, $Mn_yAs$, etc. when assisted by the temperature dependent saturation magnetization (Ms) measurements. When the samples were annealed, peaks

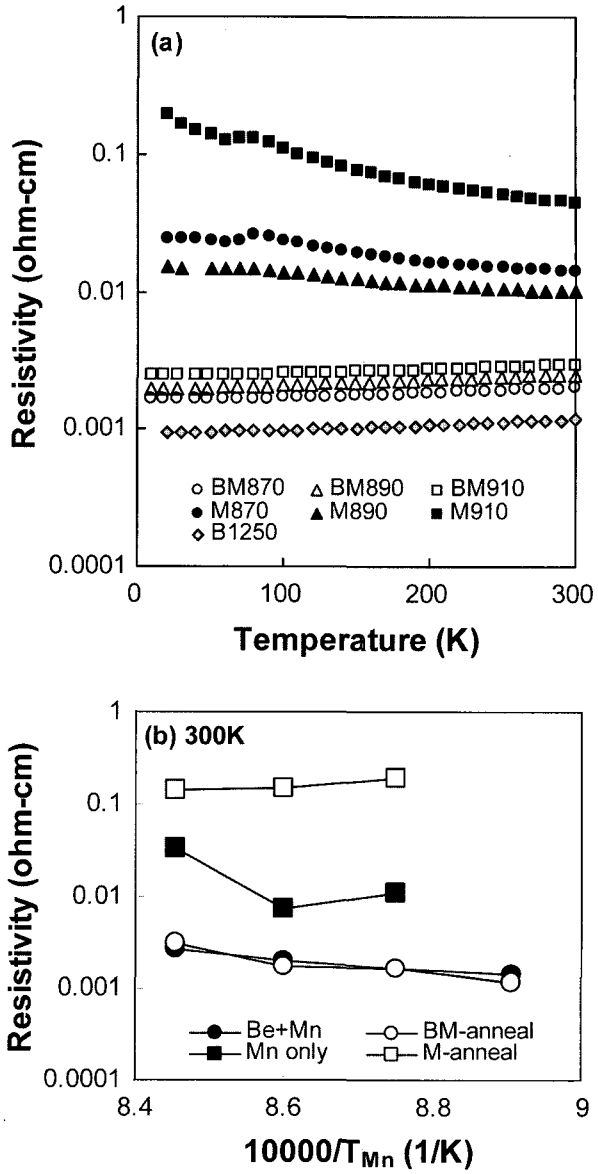


**Fig. 1.** (a) Temperature dependent resistivities of GaAs:Be, GaAs:Mn, and GaAs:(Mn,Be) layers and (b) room temperature resistivities of GaAs:Mn, and GaAs:(Mn,Be) layers grown with various Mn fluxes.

for the Mn phase have disappeared indicating that the Mn cluster is unstable at high temperature. It was shown that the interstitial Mn atoms are unstable at high temperature and relocate in GaAs lattice [11].

The temperature dependent resistivity measurements and the change of room temperature resistivity with varying Mn flux are shown in Fig. 1(a) and 1(b), respectively. The M-series layers showed the curves of semiconducting behavior with bumps indicating Tc. The resistivity is the lowest for $T_{Mn}$=890 °C and the rise for $T_{Mn}$=910 °C is due to MnAs precipitation [5]. On the

**Table 1.** Summary of the Hall-effect measurements.

| $T_{Be}$ (°C) | $T_{Mn}$ (°C) | As-grown | | | Annealed | | |
|---|---|---|---|---|---|---|---|
| | | $\rho$ ($10^{-3}$ Ω·cm) | p ($10^{19}$/cm$^3$) | $\mu$ (cm$^2$/V·s) | $\rho$ ($10^{-3}$ Ω·cm) | p ($10^{19}$/cm$^3$) | $\mu$ (cm$^2$/V·s) |
| 1250 | 870 | 1.6 | 28.0 | 13.8 | 1.6 | 19.5 | 19.6 |
| 1250 | 890 | 2.1 | 18.8 | 16.0 | 1.7 | 12.3 | 29.4 |
| 1250 | 910 | 2.7 | 25.6 | 9.1 | 3.1 | 14.1 | 14.1 |
| – | 870 | 10.8 | 6.5 | 8.9 | 192 | 0.5 | 6.4 |
| – | 890 | 7.3 | 10.7 | 7.9 | 149 | 0.5 | 9.2 |
| – | 910 | 33.6 | 4.4 | 4.2 | 139 | 0.3 | 17.6 |
| 1250 | – | 0.9 | 39.2 | 16.9 | 1.0 | 31.0 | 20.6 |

other hand, all the BM-series layers revealed metallic behavior as intended due to a degenerate codoping of Be. Recall that the metallic nature of magnetic semiconductors is a practical prerequisite for observation of magnetotransport [12]. For example, the semiconducting layer M910 (GaAs:Mn grown at $T_{Mn}$=910 °C) revealed a finite Ms from MnAs clusters, but clear magnetotransport could not be detected because of the high sheet resistance in comparison with the magnetoresistance. No clear bumps related with ferromagnetic transition could be seen at low temperatures in the BM-series exhibiting the absence of the ferromagnetic solid solution phase of GaMnAs. Instead, MnAs and MnGa precipitation was accelerated by the degenerate doping of Be as will be shown.

Hall-effect measurement results are summarized in Table 1. When the Hall-effect data of BM-series were compared with those of M-series, the mobility values were higher even at higher concentrations manifesting the superiority of Be as dopant over Mn. The hole concentration from Mn and Be in the codoped layers, however, was smaller than that in GaAs:Mn and GaAs:Be layer, respectively, due to competition for the incorporation during the growth. Actually the concentrations of Mn for the M-series samples were 0.82, 1.13, and 2.04 at% for M870, M890, and M910, respectively. The Mn concentrations have decreased with Be codoping to 0.23, 1.14, and 0.96 at% for BM870, BM890, and BM910, respectively. The anomaly in BM890 is not clear at present, but indicates a competition between Mn and Be for incorporation into the GaAs matrix during the growth. Therefore, the decreasing conductivity in the BM-series with respect to GaAs:Be (Table 1) is induced by the reduced incorporation of Be of high mobility along with the addition of Mn of low mobility as well as by the precipitates.

Thermal annealing of the layers was carried out to investigate the thermal stability of the precipitates [Fig. 1(b)]. While the film resistivity has increased upon annealing by about an order of magnitude in the M-series, the change was small in the BM-series. The resistivity is given by $1/\rho = q\mu p$, where $\rho$ is the resistivity, q the electron charge, $\mu$ the mobility, and p the hole carrier concentration. The hole concentration was decreased for both series, which are caused by Mn dopant segregation out of the GaAs matrix. This was also proved by XRD patterns. However, the segregation and subsequent precipitate formation (as observed by Ms changes) degraded the carrier mobility in the M-series, but the hole carriers dominated by Be rather enhanced the film mobility in the BM-series. While Be is thermally stable in GaAs [17], Mn atoms are unstable and redistributes to form clusters of Mn and/or MnAs in GaMnAs [11, 18]. When the electrical and magnetization properties are analyzed in connection, the degradation of film conductivity by $Mn_yAs$ is more severe than by $Mn_xGa$. This will be discussed elsewhere.

The Ms of the M- and BM-series measured by SQUID at 2 T with varying temperature is summarized in Fig. 2. The Ms comes from ferromagnetic MnAs and MnGa precipitates at least at T > ~80 K. Tc of MnAs and $Mn_xGa$ are ~310 K and higher than 600 K, respectively [19]. Although M890 and BM890 contain similar Mn concentrations (~1.1 at%), the temperature dependent Ms behavior is very different. While the negligibly small Ms value in M890 near room temperature is due to the nonmagnetic clusters of Mn, the flat Ms at low temperatures and dropping near 300 K in BM890 results from both MnAs and MnGa precipitates. The quantum theory [20] assuming two magnetic phases in the layer, MnAs (assuming $J = 5/2$) and MnGa, shows an excellent fit (solid curve). The determined Ms are 19.0 and 10.8 emu/cm$^3$ for MnAs and MnGa, respectively. It is not clear why BM910 grown at higher Mn flux shows a Ms curve dominantly of MnAs. In the meantime, the solid line for BM910 is a fitting via the quantum theory arbitrarily

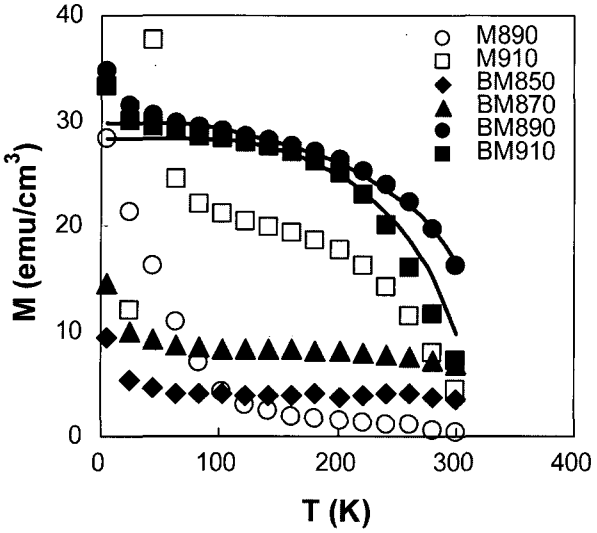


**Fig. 2.** Magnetization of GaAs:(Mn,Be) layers compared with one of GaAs:Mn layers. Theoretical fits are shown with solid curves.

using $J = 1/2$ for MnAs clusters. The quantum theory using $J = 5/2$ or the mean field theory showed poorer fits (not shown). The poorer fit with $J = 5/2$ most probably comes from the neglect of the finite amount of the existing MnGa phase in the layer.

At very high Mn flux, MnAs clusters could form without the assistance of Be as shown with M910, but MnGa phase did not form in the M-series. However, all the BM-series layers contain a finite amount of $Mn_xGa$ clusters in the as-grown state as shown in Fig. 2 and above analysis. The formation of MnGa precipitates by Be codoping can be observed even at very low Mn concentration (~0.2 at% for BM850). It was shown that the strain related with Be incorporation plays a role in stabilizing defects. The effect becomes larger in the layers grown at low temperature [17]. Thus, Be atoms provide a circumstance favorable to MnGa phase formation. The comparison between M- and BM-series suggests that Be codoping drive Mn atoms towards the formation of $Mn_xGa$ clusters. In the meantime, the study of thermal annealing showed that MnGa is thermally more stable than MnAs. Namely, MnGa phase has been more upon annealing, but MnAs phase has often decomposed. Finally, in the BM-series, Ms increases with Mn flux, but the conductivity rather decreases. Therefore, the ferromagnetism results from the ferromagnetic clusters rather than the carrier mediation enhanced by the high Be concentration. However, the highly doped GaAs matrix plays an important role in exposing the spin transport property of the clusters.

Anomalous Hall effect is a direct evidence of magneto-

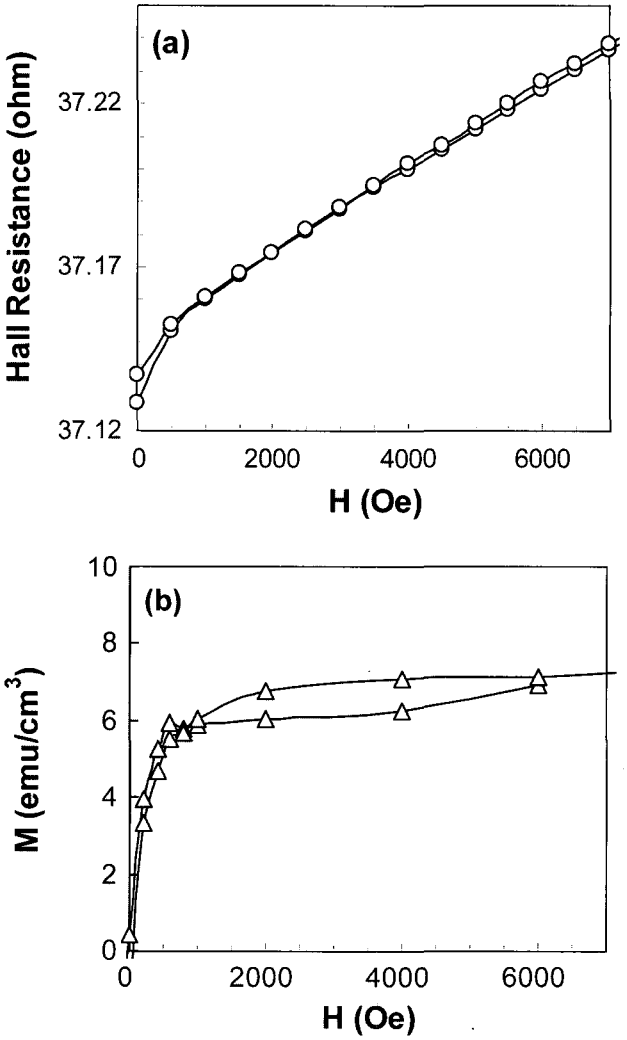


**Fig. 3.** (a) Hall resistance vs. magnetic field curve showing the anomalous Hall effect and (b) magnetization vs. magnetic field curve of the sample BM910 measured at room temperature.

transport in a structure. The anomalous Hall resistances measured on the BM-series of van der Pauw geometry are shown in Fig. 3(a). Only BM890 and BM910 having segregates revealed magnetotransport at room temperature. The Hall resistance of a magnetic film can be expressed by $tR_{Hall} = R_oB + R_SM$, where $R_o$ is the ordinary Hall coefficient, $R_S$ the anomalous Hall coefficient, and $t$ the thickness [21]. For the film in the figure, however, magnetic precipitates are distributed in a nonmagnetic matrix and form only a part of the film. Namely, $R_o$ results from the nonmagnetic matrix and the magnetic precipitates, but $R_S$ results only from the precipitates. The thickness is irrelevant to the precipitates. Therefore, the equation cannot be used to derive the characteristic parameters of the magnetic precipitates. The anomalous term from the precipitates was 0.019 ohm and is ~0.05%

of the film resistance, ~37.13 ohm. The hysteresis in the Hall resistance showed the coercivity of ~80 Oe for the precipiates. The magnetization curve at room temperature is shown in Fig. 3(b). It reveals the saturation magnetization of ~6 emu/cc. Saturations occurring at ~600 Oe can be seen in both figures. The BM-series with low Mn flux as well as all the M-series did not reveal the magnetotransport phenomena because the effect is small and should be buried in the resistance of the matrix under the sensitivity of the measurements.

Magnetotransport is a prerequisite to realization of electronic spin injection devices and it would be more useful if realized at room temperature. Since the solid solution GaMnAs is limited at ~110 K for Tc and MnAs clusters degrade the film conductivity, the observation of magnetotransport with the solid solution system may be hardly realizable. Instead, we showed that the magnetotransport of the embedded clusters of MnAs and/or MnGa could emerge through a degenerately Be doped GaAs matrix. Furthermore, the Be doping improves stabilization of the MnGa clusters. When one controls the size of the clusters, a magnetoresistance structure may be realized while maintaining the magnetic semiconductor structures.

## 4. Conclusions

The magnetotransport in GaMnAs system was realized at room temperature via formation of 1) ferromagnetic clusters whose Curie temperatures are above room temperature and 2) degenerately Be doped GaAs matrix through which the spin property can be conveyed out.

## Acknowledgments

This work was supported by the Research Center for Advanced Magnetic Materials, grant No. R01-2004-10104-0 of the Basic Research Program of KOSEF, and BK21 program, Korea. The authors also thank to Korea Basic Science Institute for the SQUID measurements.

## References

[1] Y. Ohno, D. K. Young, B. Beschoten, F. Matsukura, H. Ohno, and D. D. Awschalom, *Nature* **402**, 790 (1999).
[2] A. Shen, Y. Horikoshi, H. Ohno, and S. P. Guo, *Appl. Phys. Lett.* **71**, 1540 (1997).
[3] H. Ohno, *Science* **281**, 951 (1998).
[4] A. Shen, F. Matsukura, S. P. Guo, Y. Sugawara, H. Ohno, M. Tani, H. Abe, and H. C. Liu, *J. Crystal Growth* **201/202**, 679 (1999).
[5] H. Ohno, *J. Mag. Mag. Mater.* **200**, 110 (1999).
[6] T. Hayashi, M. Tanaka, T. Nishinaga, H. Shimada, H. Tsuchiya, and Y. Otuka, *J. Crystal Growth* **175/176**, 1063 (1997).
[7] H. Shimizu, T. Hayashi, T. Nishinaga, and M. Tanaka, *Appl. Phys. Lett.* **74**, 398 (1999).
[8] A. Van Esch, L. Van Bockstal, J. De Boeck, G. Verbanck, A.S. van Steenbergen, P. J. Wellmann, B. Grietens, R. Bogaerts, F. Herlach, and G. Borghs, *Phys. Rev.* **B56**, 13103 (1997).
[9] T. Dietl, H. Ohno, F. Matsukura, J. Cibert, and D. Ferrand, *Science* **287**, 1019 (2000).
[10] S. U. Yuldashev, H. Im, V. S. Yalishev, C. S. Park, T. W. Kang, S. Lee, Y. Sasaki, X. Liu, and J. K. Furdyna, *Appl. Phys. Lett.* **82**, 1206 (2003).
[11] K. M. Yu, W. Walukiewicz, T. Wojtowicz, W. L. Lim, X. Liu, M. Dobrowolska, and J. K. Furdyna, *Nucl. Instrum. Methods Phys. Res.* **B219-220**, 636 (2004).
[12] K. H. Kim, K. J. Lee, D. J. Kim, H. J. Kim, Y. E. Ihm, D. Djayaprawira, M. Takahashi, C. S. Kim, C. G. Kim, and S. H. Yoo, *Appl. Phys. Lett.* **82**, 1775 (2003).
[13] K. H. Kim, K. J. Lee, D. J. Kim, H. J. Kim, Y. E. Ihm, C. G. Kim, S. H. Yoo, and C. S. Kim, *Appl. Phys. Lett.* **82**, 4755 (2003).
[14] K. H. Kim, K. J. Lee, D. J. Kim, C. S. Kim, H. C. Lee, C. G. Kim, S. H. Yoo, H. J. Kim, and Y. E. Ihm, *J. Appl. Phys.* **93**, 6793 (2003).
[15] K. H. Kim, J. H. Park, B. D. Kim, C. S. Kim, D. J. Kim, H. J. Kim, and Y. E. Ihm, *Metal. Mater.* **8**, 177 (2002).
[16] A. Shen, H. Ohno, F. Matsukara, Y. Sugawara, N. Akiba, T. Koroiwa, A. Oiwa, A. Ando, S. Katsumoto, and Y. Iye, *J. Crystal Growth* **175/176**, 1069 (1997).
[17] P. Specht, M. J. Cich, R. Zhao, J. Gebauer, M. Luysberg, and E. R. Weber, *Physica* **B308-310**, 808 (2001).
[18] J. De Boeck, R. Oesterholt, A. Van Esch, H. Bender, C. Bruynseraede, C. Van Hoof, and G. Borghs, *Appl. Phys. Lett.* **68**, 2744 (1996).
[19] M. Tanaka, J. P. Harbison, J. DeBoeck, T. Sands, B. Philips, T. L. Cheeks, and V. G. Keramidas, *Appl. Phys. Lett.* **62**, 1565 (1993).
[20] B. D. Cullity in "Introduction to magnetic materials", pp. 119, Addison-Wesley, 1972.
[21] H. Ohno, F. Matsukura, A. Shen, Y. Sugawara, N. Akiba, and T. Kuroiwa, *Physica* **E2**, 904 (1998).